Published by Institute of Physics Publishing for SISSA/ISAS

Received: *January 23, 2004*
Revised: *May 17, 2004*
Accepted: *June 7, 2004*

Clone flow analysis for a theory inspired neutrino experiment planning

Andrea Donini

Dep. Física Teórica, Universidad Autonoma Madrid
E-28049 Madrid, Spain
E-mail: andrea.donini@roma1.infn.it

Davide Meloni

Dep. de Física Teórica y del Cosmos, Universidad de Granada
Campus de Fuente Nueva, E-18002 Granada, Spain
E-mail: davide.meloni@roma1.infn.it

Stefano Rigolin

Dep. Física Teórica, Universidad Autonoma Madrid
E-28049 Madrid, Spain
E-mail: stefano.rigolin@cern.ch

Abstract: The presence of several clone solutions in the simultaneous measurement of (θ_{13}, δ) has been widely discussed in literature. In this letter we write the analytical formulæ of the clones location in the (θ_{13}, δ) plane as a function of the physical input pair $(\bar{\theta}_{13}, \bar{\delta})$. We show how the clones move with changing $\bar{\theta}_{13}$. The "clone flow" can be significantly different if computed (naively) from the oscillation probabilities or (exactly) from the probabilities integrated over the neutrino flux and cross-section.
Using our complete computation we compare the clone flow of a set of possible future neutrino experiments: the CERN SuperBeam, BetaBeam and Neutrino Factory proposals. We show that the combination of these specific BetaBeam and SuperBeam does not help in solving the degeneracies. On the contrary, the combination of one of them with the Neutrino Factory Golden and Silver channel can be used, from a theoretical point of view, to solve completely the eightfold degeneracy.

Keywords: Neutrino Physics, CP violation.

JHEP06(2004)011

Contents

1. Introduction

The atmospheric and solar sector of the PMNS leptonic mixing matrix [1] have been measured with quite good resolution by SK [2], SNO [3] and KamLand [4]. These experiments measure two angles, θ_{12} and θ_{23}, and two mass differences, Δm^2_{12} and Δm^2_{23} (for the explicit form of the PMNS matrix and the adopted conventions, see for example [5]). The present bound on θ_{13}, $\sin^2\theta_{13} \leq 0.02$, is extracted from the negative results of CHOOZ [6] and from three-family analysis of atmospheric and solar data. The PMNS phase δ is totally unbounded as no experiment is sensitive to the leptonic CP violation. The main goal of next neutrino experiments will be to measure these two still unknown parameters of the leptonic mixing matrix. In this paper we concentrate on analyzing, form a theoretical point of view, a particular problem that arise when trying to measure simultaneously (θ_{13}, δ).

In [7] it has been noticed that the appearance probability $P_{\alpha\beta}(\bar\theta_{13}, \bar\delta)$ obtained for neutrinos at a fixed energy and baseline with input parameter $(\bar\theta_{13}, \bar\delta)$ has no unique solution. Indeed, the equation:

$$P_{\alpha\beta}(\bar\theta_{13}, \bar\delta) = P_{\alpha\beta}(\theta_{13}, \delta) \tag{1.1}$$

has a continue number of solutions. The locus of (θ_{13}, δ) satisfying this equation is called "equiprobability curve". Considering the equiprobability curves for neutrinos and antineutrinos with the same energy (and the same input parameters), the system of equations

$$P^{\pm}_{\alpha\beta}(\bar\theta_{13}, \bar\delta) = P^{\pm}_{\alpha\beta}(\theta_{13}, \delta) \tag{1.2}$$

(where $\pm$ refers to neutrinos and antineutrinos) has two intersections: the input pair $(\bar\theta_{13}, \bar\delta)$ and a second, energy dependent, point. This second intersection introduces an ambiguity in the measurement of the physical values of θ_{13} and δ: the so-called *intrinsic clone*. As it was made clear in [8, 9], two other sources of ambiguities are present:

- we only know the absolute value [2], $|\Delta m^2_{23}| \in [1.9, 3.5] \times 10^{-3}$ eV^2 of the atmospheric mass difference, not its sign. This ambiguity originates from the fact that atmospheric neutrino experiments measure only the leading oscillation $\nu_\mu \to \nu_\tau$ that depends quadratically on Δm^2_{23};
- we only know the allowed departure of θ_{23} from maximal mixing, $\sin^2 2\theta_{23} > 0.9$, but not if θ_{23} is actually smaller or greater than $45°$. This ambiguity originates in that neutrino experiments are looking for ν_μ, ν_e disappearance or $\nu_\mu \to \nu_\tau$ oscillation, where θ_{23} appears only through $\sin^2 2\theta_{23}$.

As a consequence, future experiments will have as ultimate goal the measure of the two continuous variables θ_{13} and δ plus the two discrete variables:

$$\bar s_{atm} = \mathrm{sign}[\Delta m^2_{23}]\,, \tag{1.3}$$

$$\bar s_{\mathrm{oct}} = \mathrm{sign}[\tan(2\theta_{23})]\,. \tag{1.4}$$

These two discrete variables assume the values ± 1, depending on the physical assignments of the Δm^2_{23} sign ($s_{\mathrm{atm}} = 1$ for $m^2_3 > m^2_2$ and $s_{\mathrm{atm}} = -1$ for $m^2_3 < m^2_2$) and of the θ_{23}-octant ($s_{\mathrm{oct}} = 1$ for $\theta_{23} < \pi/4$ and $s_{\mathrm{oct}} = -1$ for $\theta_{23} > \pi/4$). As a consequence, taking into account all the present ignorance on the neutrino mixing and masses, eq. (1.2) must be rewritten, more precisely, as:

$$P^{\pm}_{\alpha\beta}(\bar\theta_{13}, \bar\delta; \bar s_{\mathrm{atm}}, \bar s_{\mathrm{oct}}) = P^{\pm}_{\alpha\beta}(\theta_{13}, \delta; s_{\mathrm{atm}} = \bar s_{\mathrm{atm}}; s_{\mathrm{oct}} = \bar s_{\mathrm{oct}})\,, \tag{1.5}$$

where $\bar s_{\mathrm{atm}}$ and $\bar s_{\mathrm{oct}}$ have been included as input parameters in addition to $\bar\theta_{13}$ and $\bar\delta$. In eq. (1.5) we have implicitly assumed to know the right sign and the right octant for the atmospheric mass difference and angle. As these quantities are unknown (and presumably they will remain so at the time of the next neutrino facilities), all the following equiprobabilities systems of equations should be considered as well:

$$P^{\pm}_{\alpha\beta}(\bar\theta_{13}, \bar\delta; \bar s_{\mathrm{atm}}, \bar s_{\mathrm{oct}}) = P^{\pm}_{\alpha\beta}(\theta_{13}, \delta; s_{\mathrm{atm}} = -\bar s_{\mathrm{atm}}; s_{\mathrm{oct}} = \bar s_{\mathrm{oct}})\,, \tag{1.6}$$

$$P^{\pm}_{\alpha\beta}(\bar\theta_{13}, \bar\delta; \bar s_{\mathrm{atm}}, \bar s_{\mathrm{oct}}) = P^{\pm}_{\alpha\beta}(\theta_{13}, \delta; s_{\mathrm{atm}} = \bar s_{\mathrm{atm}}; s_{\mathrm{oct}} = -\bar s_{\mathrm{oct}})\,, \tag{1.7}$$

$$P^{\pm}_{\alpha\beta}(\bar\theta_{13}, \bar\delta; \bar s_{\mathrm{atm}}, \bar s_{\mathrm{oct}}) = P^{\pm}_{\alpha\beta}(\theta_{13}, \delta; s_{\mathrm{atm}} = -\bar s_{\mathrm{atm}}; s_{\mathrm{oct}} = -\bar s_{\mathrm{oct}})\,. \tag{1.8}$$

These new sets of equiprobability systems arise when we equate the true probability (left hand side) with the probabilities obtained including one of the three possible wrong guesses on s_{atm} and s_{oct} (right hand side).

Solving the four systems of eq. (1.5)–(1.8) will result in obtaining the true solution plus the appearance of additional *clones* to form an eightfold-degeneracy [9]. These eight solutions are respectively:

- the true solution and its *intrinsic clone*, obtained solving the system of eq. (1.5);
- the Δm^2_{23}-sign clones (hereafter called *sign clones*) of the true and intrinsic solution, obtained solving the system of eq. (1.6);
- the θ_{23}-octant clones (hereafter called *octant clones*) of the true and intrinsic solution, obtained solving the system of eq. (1.7);
- the $\Delta m^2_{\rm atm}$-sign θ_{23}-octant clones (hereafter called *mixed clones*) of the true and intrinsic solution, obtained solving the system of eq. (1.8).

Notice that degeneracies in oscillations have been first discussed in [10], long before being revived in [7]–[9].

In the following section we illustrate the technique used for calculating the location of the clone solutions. We describe explicitly the formulæ for the $\nu_e \to \nu_\mu$ oscillation probability, due to the great importance it has in literature. In fact this “golden” channel (together with its CP conjugate channel) has been shown to be very promising to simultaneously study the θ_{13} angle and the leptonic CP-violation at the Neutrino Factory [11, 12] and in the BetaBeam based facilities [13]. Anyway most of the considerations done apply as well to the time reversal transitions $\nu_\mu \to \nu_e$ (and the CP conjugate one) that has been considered in the context of SuperBeam facilities like the SPL CERN project [14]. The same strategy will be applied in section 3.3 to the study of the $\nu_e \to \nu_\tau$ transition (the so-called “silver channel”) at a Neutrino Factory. As pointed out in [15, 16] this channel can become very useful in reducing the number of clone solutions.

2. Probability vs number of events

Following [7, eq. (1)], the appearance probability for the $\nu_e \to \nu_\mu$ ($\bar\nu_e \to \bar\nu_\mu$) transition, expanded at second order in perturbation theory in θ_{13}, Δ_{12}/Δ_{23}, Δ_{12}/A and $\Delta_{12}L$ (see also [17, 18]), reads:

$$P^{\pm}_{e\mu}(\bar\theta_{13},\bar\delta) = X_\pm \sin^2(2\bar\theta_{13}) + Y_\pm \cos(\bar\theta_{13}) \sin(2\bar\theta_{13}) \cos\left(\pm\bar\delta - \frac{\Delta_{23}L}{2}\right) + Z\,, \tag{2.1}$$

where $\pm$ refers to neutrinos and antineutrinos, respectively. The coefficients $X^\pm, Y^\pm$ and Z are defined as follows:

$$X_\pm = \sin^2(\theta_{23}) \left(\frac{\Delta_{23}}{B_\mp}\right)^2 \sin^2\left(\frac{B_\mp L}{2}\right), \tag{2.2}$$

$$Y_\pm = \sin(2\theta_{12}) \sin(2\theta_{23}) \left(\frac{\Delta_{12}}{A}\right) \left(\frac{\Delta_{23}}{B_\mp}\right) \sin\left(\frac{AL}{2}\right) \sin\left(\frac{B_\mp L}{2}\right), \tag{2.3}$$

$$Z = \cos^2(\theta_{23}) \sin^2(2\theta_{12}) \left(\frac{\Delta_{12}}{A}\right)^2 \sin^2\left(\frac{AL}{2}\right), \tag{2.4}$$

with $A = \sqrt{2} G_F n_e$ (expressed in $\mathrm{eV}^2/\mathrm{GeV}$) and $B_\mp = |A \mp \Delta_{23}|$. Finally, $\Delta_{23} = \Delta m^2_{23}/2E_\nu$ and $\Delta_{12} = \Delta m^2_{12}/2E_\nu$. Instead of using the coefficients in eqs. (2.2)–(2.4), it is convenient [19] to introduce the following (θ_{13}, δ)-independent terms:

$$O_1^\pm = X^\pm \, , \qquad O_2^\pm = Y^\pm \cos\left(\frac{\Delta_{23} L}{2}\right) \, , \qquad O_3^\pm = Y^\pm \sin\left(\frac{\Delta_{23} L}{2}\right) \, , \qquad O_4 = Z \, . \quad (2.5)$$

Notice, however, that transition probabilities, like for example $P^\pm_{e\mu}$, are not the experimetally "measured" quantities. Experimental results are given in terms of the number of charged leptons observed in a specific detector. For the Neutrino Factory Golden channel, for example, one measures the number of interacting muons with charge opposite to those circulating in the storage ring. In a SuperBeam-driven detector the signal is, on the other hand, represented by electrons. If the considered detector can measure the lepton and hadron final energies, E_l, E_h with a good resolution, the events are then grouped in bins of energy interval ΔE_l. This is indeed the case for the proposed Magnetized Iron Calorimeter (MIC) [20] at the Neutrino Factory, where the number of muons in the i-th energy bin for the input pair $(\bar\theta_{13}, \bar\delta)$ and for a parent muon energy $\bar E_\mu$ is given by:

$$N^i_{\mu^\mp}(\bar\theta_{13}, \bar\delta) = \left\{ \frac{d\sigma_{\nu_\mu(\bar\nu_\mu)}(E_\mu, E_\nu)}{dE_\mu} \otimes P^\pm_{e\mu}(E_\nu, \bar\theta_{13}, \bar\delta) \otimes \frac{d\Phi_{\nu_e(\bar\nu_e)}(E_\nu, \bar E_\mu)}{dE_\nu} \right\}_{E_i}^{E_i + \Delta E_\mu} \, , \quad (2.6)$$

where $\otimes$ stands for a convolution integral [15]. The same happens for the Emulsion Cloud Chamber (ECC) [16] (see Sect. 3.3 for details). On the contrary, whenever the considered detector energy resolution is not sufficient to group events in bins of energy, one single sample will be considered. This is for example the case for the Water Cherenkov detector located at the Frejus as the target of a SuperBeam (SB) or Beta-Beam (BB) experiments, as we can read from [13].

Using the O_j coefficients in eq. (2.5) we define the following integrals:

$$I_j^\pm = \left\{ \frac{d\sigma_{\nu_\mu(\bar\nu_\mu)}(E_\mu, E_\nu)}{dE_\mu} \otimes O_j^\pm(E_\nu) \otimes \frac{d\Phi_{\nu_e(\bar\nu_e)}(E_\nu, \bar E_\mu)}{dE_\nu} \right\}_{E_i}^{E_i + \Delta E_\mu} \, , \quad (2.7)$$

where the O_j coefficients are convoluted over the νN cross-section and the differential neutrino flux. All the experimental details, such as the flux shape, the cross-section, the baseline and the solar, atmospheric and matter parameters are encoded in these integrals. The number of events in the i-th bin, in the same approximation used for eqs. (2.1), is therefore:[1]

$$\begin{aligned} N^i_{\mu^-} &= \left\{ I_1^+ \sin^2(2\theta_{13}) + \left[I_2^+ \cos\delta + I_3^+ \sin\delta \right] \cos\theta_{13} \sin(2\theta_{13}) + I_4^+ \right\}^i \, , \\ N^i_{\mu^+} &= \left\{ I_1^- \sin^2(2\theta_{13}) + \left[I_2^- \cos\delta - I_3^- \sin\delta \right] \cos\theta_{13} \sin(2\theta_{13}) + I_4^- \right\}^i \, . \end{aligned} \quad (2.8)$$

[1]Notice that a possible difference between I_4^+ and I_4^- can be induced by different neutrino and antineutrino fluxes and/or cross-sections, not by the coefficient O_4 that is identical for neutrinos and antineutrinos.

For a specific energy bin and fixed input parameters $(\bar\theta_{13}, \bar\delta)$, we derive the clone location in the (θ_{13}, δ) plane solving:

$$N^i_{\mu^\pm}(\bar\theta_{13}, \bar\delta; \bar s_{\rm atm}, \bar s_{\rm oct}) = N^i_{\mu^\pm}(\theta_{13}, \delta; s_{\rm atm} = \bar s_{\rm atm}, s_{\rm oct} = \bar s_{\rm oct}) \tag{2.9}$$
$$N^i_{\mu^\pm}(\bar\theta_{13}, \bar\delta; \bar s_{\rm atm}, \bar s_{\rm oct}) = N^i_{\mu^\pm}(\theta_{13}, \delta; s_{\rm atm} = \bar s_{\rm atm}, s_{\rm oct} = -\bar s_{\rm oct}) \tag{2.10}$$
$$N^i_{\mu^\pm}(\bar\theta_{13}, \bar\delta; \bar s_{\rm atm}, \bar s_{\rm oct}) = N^i_{\mu^\pm}(\theta_{13}, \delta; s_{\rm atm} = -\bar s_{\rm atm}, s_{\rm oct} = \bar s_{\rm oct}) \tag{2.11}$$
$$N^i_{\mu^\pm}(\bar\theta_{13}, \bar\delta; \bar s_{\rm atm}, \bar s_{\rm oct}) = N^i_{\mu^\pm}(\theta_{13}, \delta; s_{\rm atm} = -\bar s_{\rm atm}, s_{\rm oct} = -\bar s_{\rm oct}) \tag{2.12}$$

as it was the case for the transition probability in eqs. (1.5)–(1.8).

3. Location of the clones

In this section we determine the analytic expression for the clone location, in the case of $\nu_e \to \nu_\mu$ oscillations, solving the integrated systems in eqs. (2.9)–(2.12). We are first going to describe in detail the procedure for calculating the *intrinsic* clone and then we present, for all the cases, the simplified vacuum formulæ. A detailed derivation is deferred to appendix A. Moreover, in order to simplify the notation, from now on we will omit any reference to the bin index i in the convolution integrals, eq. (2.7).

The results of this section apply for identical neutrino/antineutrino fluxes and approximately constant cross-sections (such as in the case of the Neutrino Factory).

3.1 The intrinsic clone

We derive now the theoretical solution of eq. (2.9) following the outline of [15]. This equation corresponds to the particular case $s_{\rm atm} = \bar s_{\rm atm}; s_{\rm oct} = \bar s_{\rm oct}$. The explicit results that we get for δ and θ_{13} can be compared with [7, 15].

Eq. (2.9) draws two continuous equal-number-of-events (ENE) lines in the (θ_{13}, δ) plane. We derive an implicit equation in δ:

$$F^\pm(\delta) = G^\pm(\theta_{13}, \bar\theta_{13}, \bar\delta)\,, \tag{3.1}$$

where

$$F^\pm(\delta) = \cos\delta \pm \left(\frac{I_3^\pm}{I_2^\pm}\right)\sin\delta \tag{3.2}$$

and

$$G^\pm(\theta_{13}, \bar\theta_{13}, \bar\delta) = \left(\frac{I_1^\pm}{I_2^\pm}\right) f(\theta_{13}, \bar\theta_{13}) + F^\pm(\bar\delta)\, g(\theta_{13}, \bar\theta_{13})\,. \tag{3.3}$$

The two θ_{13}-dependent functions, f and g, are:

$$\left\{\begin{aligned} f(\theta_{13}, \bar\theta_{13}) &= \frac{\sin^2(2\bar\theta_{13}) - \sin^2(2\theta_{13})}{\cos\theta_{13}\sin(2\theta_{13})} \\ g(\theta_{13}, \bar\theta_{13}) &= \frac{\cos\bar\theta_{13}\sin(2\bar\theta_{13})}{\cos\theta_{13}\sin(2\theta_{13})} \end{aligned}\right. \tag{3.4}$$

This parametrization is valid for any value of $\bar\theta_{13}$, including $\bar\theta_{13} \to 0$: not an irrelevant feature, since even in the case of vanishing $\bar\theta_{13}$ clone solutions with a non null value of

θ_{13} can appear. In this case a totally wrong conclusion about the value of $\bar{\theta}_{13}$ can indeed originate by a naive analysis of the experimental results. Notice, finally, the trivial limits $f(\bar{\theta}_{13},\bar{\theta}_{13})=0$ and $g(\bar{\theta}_{13},\bar{\theta}_{13})=1$.

Solving the system in eq. (3.1), we derive two equations for $\sin\delta$ and $\cos\delta$:

$$\begin{aligned}\sin\delta &= C\, f(\theta_{13},\bar{\theta}_{13}) + g(\theta_{13},\bar{\theta}_{13})\ \sin\bar{\delta}\\ \cos\delta &= D\, f(\theta_{13},\bar{\theta}_{13}) + g(\theta_{13},\bar{\theta}_{13})\ \cos\bar{\delta}\end{aligned} \tag{3.5}$$

where the coefficients are

$$C = \left[\frac{I_1^+ I_2^- - I_1^- I_2^+}{I_3^+ I_2^- + I_3^- I_2^+}\right], \qquad D = \left[\frac{I_1^+ I_3^- + I_1^- I_3^+}{I_3^+ I_2^- + I_3^- I_2^+}\right]. \tag{3.6}$$

In the following results, the baseline and energy bin dependence appears only through these integral ratios. Notice that only three of the four integrals $I_j^\pm$ are present in C and D. In fact, there is no dependence on I_4 due to the fact that for $s_{\rm oct} = \bar{s}_{\rm oct}$ this integral drops between left and right hand sides of eq. (2.8).

In the approximation $\cos\theta_{13} \simeq \cos\bar{\theta}_{13} \simeq 1$, perfectly valid since $\theta_{13} \leq 10^\circ$ [6], we solve eq. (3.5) for θ_{13} to get:

$$\sin^2 2\theta_{13} = \begin{cases} \sin^2 2\bar{\theta}_{13} \\ \sin^2 2\bar{\theta}_{13} + \dfrac{1 + 2\left[D\cos\bar{\delta} + C\sin\bar{\delta}\right]\sin 2\bar{\theta}_{13}}{C^2 + D^2}\end{cases} \tag{3.7}$$

in which the first solution represents the true input value $\theta_{13} = \bar{\theta}_{13}$ and the second one the location of the intrinsic clone. Eventually, substituting the results of eq. (3.7) into $f(\theta_{13},\bar{\theta}_{13})$ and $g(\theta_{13},\bar{\theta}_{13})$, we can get the value of δ for the intrinsic clone using one of the relations in eq. (3.5).

It is interesting to specialize these results to the case of very short baseline L, where matter effects can be neglected. In the vacuum approximation, the convolution integrals of the four O_j coefficients no longer differ for neutrinos and antineutrinos, $\lim_{A\to 0} I_j^\pm = I_j$. As a consequence,

$$\lim_{A\to 0} C = 0 \qquad \lim_{A\to 0} D = \frac{I_1}{I_2} \tag{3.8}$$

and

$$\begin{aligned}\sin\delta &= g(\theta_{13},\bar{\theta}_{13})\ \sin\bar{\delta}\\ \cos\delta &= \frac{I_1}{I_2}\, f(\theta_{13},\bar{\theta}_{13}) + g(\theta_{13},\bar{\theta}_{13})\ \cos\bar{\delta}\,.\end{aligned} \tag{3.9}$$

The location of the intrinsic clone in vacuum is:

$$\sin^2 2\theta_{13} = \sin^2 2\bar{\theta}_{13} + \left(\frac{I_2}{I_1}\right)^2 \left[1 + 2\left(\frac{I_1}{I_2}\right)\cos\bar{\delta}\ \sin 2\bar{\theta}_{13}\right]. \tag{3.10}$$

Notice that in vacuum the clone location depends on I_1 and I_2, only: the dependence on I_3 has also dropped from eq. (3.9). Eq. (3.10) generalizes the results of [7] and [14], where two regimes ("atmospheric" and "solar", for large and small $\bar\theta_{13}$, respectively) are discussed independently. In particular, at first order in I_2/I_1 our vacuum solution for θ_{13} reproduces [14, eq. (5)], valid in the atmospheric regime:

$$\sin^2 2\theta_{13} \simeq \sin^2 2\bar\theta_{13} + 2\frac{I_2}{I_1}\cos\bar\delta\,\sin 2\bar\theta_{13} \tag{3.11}$$

$$\cot\delta \simeq -\cot\bar\delta - \frac{I_2}{I_1}\frac{1}{\sin 2\bar\theta_{13}\,\sin\bar\delta} \tag{3.12}$$

For values of $\bar\theta_{13}$ large enough, $\delta \sim \pi - \bar\delta + \mathcal{O}(I_2/I_1)$.

3.2 Of other clones

The general case is represented by eq. (2.12). In this case, integrals on left and right hand side of eq. (2.8) are different and we can no longer factorize easily the θ_{13} dependence. As a consequence, the notation is going to be more involved with respect to the intrinsic case. To gain analytical insight of the results, however, we can carry on a bit more our mathematical manipulation. We label as $\bar I_j$ the true integrals (on left hand side of eq. (2.8)) and I_j those to be determined in the experiment (on right hand side of eq. (2.8)). We modify the functions in eq. (3.4) as follows:

$$\begin{cases} f'_\pm(\theta_{13},\bar\theta_{13}) &= \dfrac{\sin^2(2\bar\theta_{13}) - [I_1^\pm/\bar I_1^\pm]\sin^2(2\theta_{13})}{\cos\theta_{13}\sin(2\theta_{13})}\,, \\ h'(\theta_{13}) &= \left(1-\dfrac{I_4}{\bar I_4}\right)\dfrac{1}{\cos\theta_{13}\sin(2\theta_{13})}\,, \end{cases} \tag{3.13}$$

with $f'_\pm(\theta_{13},\bar\theta_{13}) = f(\theta_{13},\bar\theta_{13})$ and $h'(\theta_{13}) = 0$ in the intrinsic case.

With these definitions we can rewrite eq. (3.3) as follows:

$$G^\pm(\theta_{13},\bar\theta_{13},\bar\delta) = \left[\frac{\bar I_1^\pm}{I_2^\pm} f'_\pm(\theta_{13},\bar\theta_{13}) + \frac{\bar I_2^\pm}{I_2^\pm}\bar F^\pm(\bar\delta) g(\theta_{13},\bar\theta_{13}) + \frac{\bar I_4}{I_2^\pm} h'(\theta_{13})\right], \tag{3.14}$$

where, clearly,

$$\bar F^\pm(\delta) = \cos\delta \pm \left(\frac{\bar I_3^\pm}{\bar I_2^\pm}\right)\sin\delta\,. \tag{3.15}$$

In table 1 we present the relation between the $\bar I_j$ true integrals and those that undergo a discrete $s_{\rm atm}$ and/or $s_{\rm oct}$ transformation. As it can be seen, the effect of $s_{\rm atm} \to -s_{\rm atm}$ is to flip neutrinos with antineutrinos (notice that I_4 is unaffected by this change). The change in the θ_{23} octant introduces a dependence on θ_{23} in I_1 and I_4, leaving $I_{2,3}$ unmodified. Using table 1, we can specialize eq. (3.14) for the three ambiguities and derive analytical results for the *sign, octant* and *mixed* clones. These results are typically rather cumbersome and we refer the interested reader to Appendix A for the explicit analytical formulæ for the different clone locations.

We specialize here to the vacuum case. In this case, since the convolution integrals make no distinction between neutrinos and antineutrinos, the transformation properties of Tab. 1 simplify considerably. In particular, I_3 is unaffected by any of the discrete transformation; I_2 changes sign when $s_{\rm atm} \to -s_{\rm atm}$ and is unaffected by an octant shift;

JHEP06(2004)011

	Intrinsic: $s_{\rm atm} = \bar{s}_{\rm atm}$ $s_{\rm oct} = \bar{s}_{\rm oct}$	Octant: $s_{\rm atm} = \bar{s}_{\rm atm}$ $s_{\rm oct} = -\bar{s}_{\rm oct}$	Sign: $s_{\rm atm} = -\bar{s}_{\rm atm}$ $s_{\rm oct} = \bar{s}_{\rm oct}$	Mixed: $s_{\rm atm} = -\bar{s}_{\rm atm}$ $s_{\rm oct} = -\bar{s}_{\rm oct}$
$I_1^\pm$	$\bar{I}_1^\pm$	$\cot^2(\theta_{23})\, \bar{I}_1^\pm$	$\bar{I}_1^\mp$	$\cot^2(\theta_{23})\, \bar{I}_1^\mp$
$I_2^\pm$	$\bar{I}_2^\pm$	$\bar{I}_2^\pm$	$-\bar{I}_2^\mp$	$-\bar{I}_2^\mp$
$I_3^\pm$	$\bar{I}_3^\pm$	$\bar{I}_3^\pm$	$\bar{I}_3^\mp$	$\bar{I}_3^\mp$
I_4	$\bar{I}_4$	$\tan^2(\theta_{23})\, \bar{I}_4$	$\bar{I}_4$	$\tan^2(\theta_{23})\, \bar{I}_4$

Table 1: Transformation laws of the integrals I_j under the discrete ambiguities in the θ_{23} octant and in the Δm^2_{23} sign.

I_1 and I_4 are unaffected by changes of $s_{\rm atm}$, whereas get a θ_{23} dependence for an $s_{\rm oct}$ change. Notice that for $\theta_{23} = 45°$, only I_2 is sensitive to the sign of Δm^2_{23}.

The vacuum limit of eq. (3.13) is given by:

- *Intrinsic and sign clone*

$$\begin{cases} f'_\pm(\theta_{13}, \bar{\theta}_{13}) \to f(\theta_{13}, \bar{\theta}_{13}) \\ h'(\theta_{13}) \qquad\quad \to 0 \end{cases} \tag{3.16}$$

- *Octant and mixed clone*

$$\begin{cases} f'_\pm(\theta_{13}, \bar{\theta}_{13}) \to f'_0(\theta_{13}, \bar{\theta}_{13}) = \dfrac{\sin^2(2\bar{\theta}_{13}) - \cot^2\theta_{23}\sin^2(2\theta_{13})}{\cos\theta_{13}\sin(2\theta_{13})}\,, \\ h'(\theta_{13}) \qquad\quad \to h'_0(\theta_{13}) = \left(1 - \tan^2\theta_{23}\right) \dfrac{1}{\cos\theta_{13}\sin(2\theta_{13})}\,, \end{cases} \tag{3.17}$$

Eq. (3.9) for $\sin\delta$ becomes in vacuum:

$$\sin\delta = g(\theta_{13}, \bar{\theta}_{13})\ \sin\bar{\delta} \tag{3.18}$$

for all the four clones. The equation for $\cos\delta$ in vacuum is, on the other hand, different in the four cases:

- *Intrinsic clone*: $(\cos\delta)_{\rm int} = \dfrac{\bar{I}_1}{\bar{I}_2}\, f(\theta_{13}, \bar{\theta}_{13}) + g(\theta_{13}, \bar{\theta}_{13}) \cos\bar{\delta}$
- *Sign clone*: $(\cos\delta)_{\rm sign} = -(\cos\delta)_{\rm int}$
- *Octant clone*: $(\cos\delta)_{\rm oct} = \dfrac{\bar{I}_1}{\bar{I}_2}\, f'_0(\theta_{13}, \bar{\theta}_{13}) + g(\theta_{13}, \bar{\theta}_{13}) \cos\bar{\delta} + \dfrac{\bar{I}_4}{\bar{I}_2}\, h'_0(\theta_{13})$
- *Mixed clone*: $(\cos\delta)_{\rm mixed} = -(\cos\delta)_{\rm oct}$.

Since the only difference for intrinsic and sign clones and for octant and mixed ones is a sign in front of the $\cos\delta$ equation, we only get two vacuum solutions:

JHEP06(2004)011

- *Intrinsic and sign clones*

$$\sin^2 2\theta_{13} = \begin{cases} \sin^2 2\bar\theta_{13} \\ \sin^2 2\bar\theta_{13} + \left(\dfrac{\bar I_2}{\bar I_1}\right)^2 \left[1 + 2\left(\dfrac{\bar I_1}{\bar I_2}\right)\cos\bar\delta \, \sin 2\bar\theta_{13}\right] \end{cases} \tag{3.19}$$

- *Octant and mixed clones*

$$\begin{aligned} \sin^2 2\theta_{13} = & \sin^2 2\bar\theta_{13} + \\ & + \left\{ \tan^2\theta_{23} \frac{\bar I_2}{\bar I_1} \left[\cos\bar\delta \sin 2\bar\theta_{13} + \tan^2\theta_{23} \frac{\bar I_2}{2\bar I_1}\right] - \left(1 - \tan^2\theta_{23}\right) \times \right. \\ & \left. \times \left(\sin^2 2\bar\theta_{13} - \tan^2\theta_{23} \frac{\bar I_4}{\bar I_1}\right)\right\} \pm \\ & \pm \tan^2\theta_{23} \frac{\bar I_2}{\bar I_1} \left\{ \left[\cos\bar\delta \, \sin 2\bar\theta_{13} + \tan^2\theta_{23}\frac{\bar I_2}{2\bar I_1}\right]^2 - \left(1 - \tan^2\theta_{23}\right) \times \right. \\ & \left. \times \left(\sin^2 2\bar\theta_{13} - \tan^2\theta_{23}\frac{\bar I_4}{\bar I_1}\right)\right\}^{1/2} . \end{aligned} \tag{3.20}$$

Notice that for the intrinsic and sign clones in vacuum, one solution is the true solution $\theta_{13} = \bar\theta_{13}$ whereas the second solution get shifted with respect to $\bar\theta_{13}$. This is not the case for the octant and mixed clones that, also in the vacuum limit, will undergo a shift with respect to $\bar\theta_{13}$ for both solutions. Eq. (3.19) can be immediately recovered from eq. (3.20) for $\theta_{23} = 45^\circ$.

The solution for the clone location along the δ axis can be found using eq. (3.18). Notice that, due to property of the vacuum transition probabilities under a change in the sign of Δm^2_{23}, the δ shift for the sign and mixed clones is obtained replacing $\delta_{\rm sign} = \pi - \delta_{\rm int}$ and $\delta_{mixed} = \pi - \delta_{\rm oct}$.

3.3 The $\nu_e \to \nu_\tau$ transition

The results of Sect. 3.1 and 3.2 can be straightforwardly extended to the $\nu_e \to \nu_\tau$ oscillations. In the same approximation used for eq. (2.1), we get for the oscillation probability:

$$P^{\pm}_{e\tau}(\bar\theta_{13}, \bar\delta) = X^\tau_\pm \sin^2(2\bar\theta_{13}) - Y_\pm \cos(\bar\theta_{13}) \sin(2\bar\theta_{13}) \cos\left(\pm\bar\delta - \frac{\Delta_{23} L}{2}\right) + Z^\tau , \tag{3.21}$$

with the following coefficients:

$$X^\tau_\pm = \cos^2(\theta_{23}) \left(\frac{\Delta_{23}}{B_\mp}\right)^2 \sin^2\left(\frac{B_\mp L}{2}\right), \tag{3.22}$$

$$Z^\tau = \sin^2(\theta_{23}) \sin^2(2\theta_{12}) \left(\frac{\Delta_{12}}{A}\right)^2 \sin^2\left(\frac{AL}{2}\right). \tag{3.23}$$

The coefficient $Y_\pm$ is defined in eq. (2.3), and it appears multiplied by a factor (-1) with respect to the same term in eq. (2.1). The different correlation between θ_{13} and δ due to this sign has been shown to offer a possible solution of the intrinsic ambiguity at a Neutrino Factory, [15, 16].

Eq. (2.6) must be modified to take into account the $\tau \to \mu$ branching ratio and the energy distribution of muons proceeding from a τ-decay. The number of wrong-sign muons in the detector is therefore:

$$
\begin{aligned}
N_{\mu^\mp}(\bar\theta_{13},\bar\delta) \;=\; BR(\tau\to\mu)\Bigg\{ \left[\frac{dN_{\mu^\mp}(E_\mu,E_\tau)}{dE_\mu} \otimes \frac{d\sigma_{\nu_\tau(\bar\nu_\tau)}(E_\tau,E_\nu)}{dE_\tau}\right] \otimes P^{\pm}_{e\tau}(E_\nu,\bar\theta_{13},\bar\delta) \otimes \\
\otimes \frac{d\Phi_{\nu_e(\bar\nu_e)}(E_\nu,\bar E_\mu)}{dE_\nu}\Bigg\}_{E_i}^{E_i+\Delta E_\mu} .
\end{aligned}
$$

The integrals I^τ_j are consequently:

$$
\begin{aligned}
I_j \;=\; BR(\tau\to\mu)\Bigg\{ \left[\frac{dN_{\mu^\mp}(E_\mu,E_\tau)}{dE_\mu} \otimes \frac{d\sigma_{\nu_\tau(\bar\nu_\tau)}(E_\tau,E_\nu)}{dE_\tau}\right] \otimes \\
\otimes\, O^{\pm}_j(E_\nu) \otimes \frac{d\Phi_{\nu_e(\bar\nu_e)}(E_\nu,\bar E_\mu)}{dE_\nu}\Bigg\}_{E_i}^{E_i+\Delta E_\mu} .
\end{aligned}
\tag{3.24}
$$

The analytic results of section 3.1 and 3.2 are formally extended to the $\nu_e \to \nu_\tau$ oscillation replacing the I^μ_j with I^τ_j as follows:

$$
\begin{cases}
I^\mu_1 \to \tan^2\theta_{23} I^\tau_1 \\
I^\mu_2 \to -I^\tau_2 \\
I^\mu_3 \to -I^\tau_3 \\
I^\mu_4 \to \cot^2\theta_{23} I^\tau_4 \,.
\end{cases}
\tag{3.25}
$$

4. The degeneracies flow

In this section we will apply our analytic results to illustrate, from a theoretical point of view, where the different clones of the true solution, $(\bar\theta_{13},\bar\delta)$, are located in the (θ_{13},δ) plane for different experiments that have been discussed in the literature. The goal is to show which combination of experiments is better suited to solve some (or all) of the degeneracies. Notice that the existence of unresolved degeneracies could, in fact, manifests itself in a complete lost of predictability on the aforementioned parameters. It must be noticed that this analysis only provides a useful tool to detect the experiment synergies that are most promising to measure these two still unknown entries of the PMNS matrix. These results must then be confirmed by a detailed analysis in which statistics and systematics of a given experiment combination are carefully taken into account. This experimental analysis is well beyond the scope of this paper where we only focus in giving a theoretical insight of the problem.

The experiments that we have considered in our analysis are the following:

- A Neutrino Factory with 50 GeV muons circulating in the storage ring and two detectors: the first one located at $L = 2810$ Km is designed to look for the golden channel (hereafter labeled as NFG); the second one located at $L = 732$ Km is designed to look for the silver channel (hereafter labeled as NFS). The average neutrino energy is: $\langle E_{\nu_e,\bar\nu_e}\rangle \simeq 30$ GeV.

- A SuperBeam with 2 GeV protons and one detector located at $L = 130$ Km to look for $\nu_\mu \to \nu_e$ (hereafter labeled as SB). The average neutrino energy is: $\langle E_{\nu_\mu} \rangle \simeq 270$ MeV and $\langle E_{\bar{\nu}_\mu} \rangle \simeq 250$ MeV.

- A Beta Beam with ^{6}He and ^{18}Ne ions and one detector located at $L = 130$ Km to look for $\nu_e \to \nu_\mu$ (hereafter labeled as BB). The average neutrino energy is: $\langle E_{\nu_e} \rangle \simeq 360$ MeV and $\langle E_{\bar{\nu}_e} \rangle \simeq 240$ MeV.

Notice that for our theoretical analysis the details of the detectors (such as the mass or the specific technology adopted to look for a given signal) are irrelevant, since they cancel between left and right hand side of eqs. (2.9)–(2.12). However, the relevant parameters (the neutrino fluxes and the baseline) have been chosen considering the following proposed experiments: [11, 20] (NFG), [15, 16] (NFS), [21] (SB) and [13] (BB). For the different beams we have taken as representative the CERN Neutrino Factory, SPL and BetaBeam proposals.[2].

The input parameters used in the computation are:

- The Atmospheric Sector: $\Delta m^2_{23} = 2.5 \times 10^{-3}\,\text{eV}^2$, $\theta_{23} = 40°$;

- The Solar Sector: $\Delta m^2_{12} = 7.3 \times 10^{-5}\,\text{eV}^2$, $\theta_{12} = 35°$;

- The Matter Parameter: $A = 1.1 \times 10^{-4}\,\text{eV}^2/\text{GeV}$.

The theoretical requirement for solving ambiguities is to find a specific combination of experiments such that the corresponding clone flows lie "well apart". In this scenario an experimental fit to the data will result in a good χ^2 absolute minimum near the true solution, where the information from different experiments adds coherently. Near the theoretical clone locations poor χ^2 relative minima will be found, since in these points the results of different experiments do not add coherently.

In section 4.1 we compare the clone locations derived from equiprobability and ENE curves; in section 4.2.1 we consider the intrinsic and the sign clones; in section 4.2.2 we focus on the octant and the mixed clones. We have shown in section 3.2 that the two pairs of solutions are indeed related in the vacuum limit.

4.1 Equiprobability flow vs ENE flow

From a theoretical point of view one can look at the clone displacement with respect to the true solution ($\theta_{13} = \bar{\theta}_{13}$, $\delta = \bar{\delta}$) solving either the systems for the equiprobability curves, eqs. (1.5)–(1.8), or the corresponding systems for the ENE curves, eqs. (2.9)–(2.12). One should expect the two treatments to be equivalent: this is not always the case.

In figure 1 we plot the location of the intrinsic clone that results from the equiprobability curves and from the ENE curves in the particular case $\bar{\delta} = 90°$ for variable input parameter $\bar{\theta}_{13}$ in the range $\bar{\theta}_{13} \in [0.1°, 10°]$. These points graphically depict how far from the true solution the degeneracy falls. A small change in the input parameter $\bar{\theta}_{13}$ results in a small shift of the clone location (remind, however, the 2π-periodicity in the δ axis).

[2]See for example in [22] for a detailed description of each of these proposals.

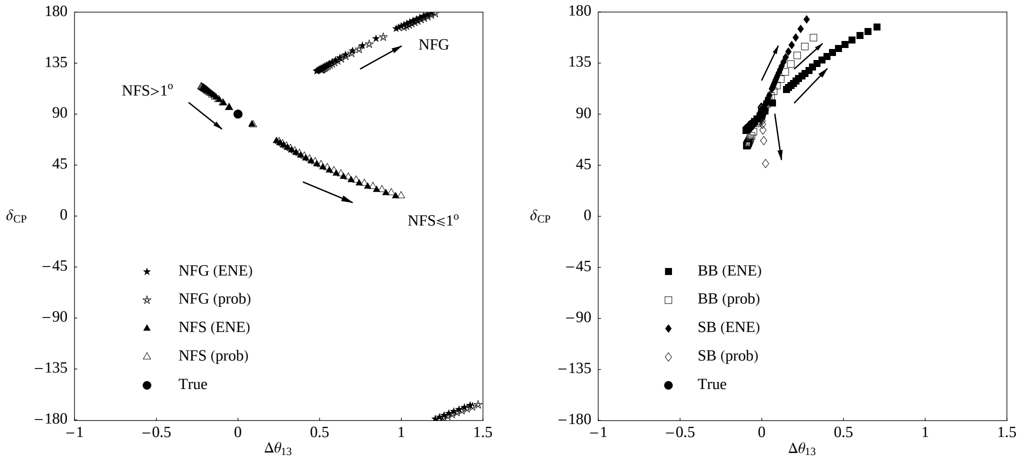

Figure 1: Intrinsic clone flow for the Neutrino Factory golden and silver channels (left) and the SuperBeam and BetaBeam signals (right), in the $(\Delta\theta_{13}, \delta)$ plane for $\bar\theta_{13} \in [0.1°, 10°], \bar\delta = 90°$. The full circle is the true solution. The full (empty) symbols represent the intrinsic clone flow, computed from the ENE (equiprobability) curves.

Almost continuous geometrical regions where degeneracies lie are therefore defined for a given interval in $\bar\theta_{13}$, illustrating how the clones move due to a change in the input parameters: we will call this the "clone flow". In the left plot we present the results for the Neutrino Factory-based golden and silver channels (i.e. $\nu_e \to \nu_\mu, \nu_\tau$), whereas in the right plot those of a SuperBeam-based $\nu_\mu \to \nu_e$ and of a BetaBeam-based $\nu_e \to \nu_\mu$ signals. The arrows describe the direction of the flows: from large to small $\bar\theta_{13}$. The plots should be read as follows:

- the horizontal axis is $\Delta\theta_{13} = \theta_{13} - \bar\theta_{13}$. This is the value of the θ_{13}-shift, as derived in the second solution of eq. (3.7);
- the vertical axis is the CP-violating phase δ itself, as it can be derived introducing the result of eq. (3.7) into one of eqs. (3.5).

For any value of the input parameter $\bar\theta_{13}$ the true solution is represented by the full (black) circle in $\Delta\theta_{13} = 0$, $\delta = \bar\delta = 90°$. Notice that this property is specific to the intrinsic case. In general, both solutions of eqs. (2.10)–(2.12) will differ from the true solution $(\bar\theta_{13}, \bar\delta)$. The intrinsic clones, computed using the ENE or the equiprobability equations, are respectively plotted as full or empty symbols as explained in the legend and in the caption.

In the left plot of figure 1 we can clearly identify the golden and silver channel intrinsic clone flow.[3] The NFG flow goes from the true solution toward positive $\Delta\theta_{13}$ and positive $\delta - \bar\delta$: for $\bar\theta_{13} = 10°$ we have $\Delta\theta_{13} \sim 0.5°$ and for very small $\bar\theta_{13}$, $\Delta\theta_{13} \to 1.5°$.

[3]For this specific plot we are choosing the energy bin between $30-40$ GeV but the same conclusion holds for all the other bins as well for the integrated flux.

The NFS flow goes from negative $\Delta\theta_{13}$ and positive $\delta - \bar{\delta}$ toward positive $\Delta\theta_{13}$ and negative $\delta - \bar{\delta}$. The different behavior of the two flows reflects the results of eq. (3.7). For $\nu_e \to \nu_\mu$ transitions, the second solution of eq. (3.7) gives $\sin^2 2\theta_{13} \geq \sin^2 2\bar{\theta}_{13}$ for any value of $\bar{\theta}_{13}$, being C and D strictly positive quantities. On the contrary, due to the formal replacement of the convolution integrals $I_2^\mu \to -I_2^\tau, I_3^\mu \to -I_3^\tau$ we find that C^τ, D^τ are strictly negative quantities. For changing $\bar{\theta}_{13}$, therefore, the θ_{13}-shift can either be positive or negative. Notice how the intrinsic flows computed from the integrated ENE curves and from the equiprobability curves (almost) coincide for the Neutrino Factory-based samples.

In the right plot of figure 1 SuperBeam and BetaBeam-based flows are shown. The ENE clone flow for the SB facility (full diamonds) shows a very small $\Delta\theta_{13}$ for any value of $\bar{\theta}_{13}$. The δ-shift goes from negative for large $\bar{\theta}_{13}$ to positive for small $\bar{\theta}_{13}$, approaching $\delta = 180^\circ$ for $\bar{\theta}_{13} \to 0$. The ENE flow for the BB facility (full squares) is qualitatively similar to the SB one.

The important feature is that for both facilities the difference between using ENE (full symbols) or equiprobability (empty symbols) curves is significantly larger than in the case of Neutrino Factory flows discussed before. In particular, notice how the SB intrinsic clone computed from equiprobability curves flows towards $\delta = 0$ for $\bar{\theta}_{13} \to 0$, in striking contrast with the results obtained from the ENE curves. Using theoretical information from the equiprobability curves could thus lead to largely wrong conjectures. The reason why SB and BB present this large difference between the two treatments has to be searched in their narrow energy spectrum. For very peaked spectra the approximation of "constant flux", that is implicit in the equiprobability curves, badly fails. On the other hand, the broad neutrino spectrum from a Neutrino Factory makes the two treatments practically equivalent.

The theoretical results obtained for the intrinsic clone are quite general: a large difference in computing the clone location from ENE or equiprobability curves is observed for narrow band beam experiments, whereas no difference is observed for broad band beam experiments. For this reason, in the following sections we will compute the clone location for the different experiments using the integrated ENE curves.

4.2 ENE flows for different facilities

In this section we analyse the flows of the different degeneracies for the four considered facilities. We compute the theoretical clone locations for a variable $\bar{\theta}_{13}$ in the range $\bar{\theta}_{13} \in [0.1^\circ, 10^\circ]$, going from the present CHOOZ upper bound $[\sin^2 2\bar{\theta}_{13}]_{\max} = \mathcal{O}(10^{-1})$ down to $[\sin^2 2\bar{\theta}_{13}]_{\min} = \mathcal{O}(10^{-5})$. Notice that the sensitivity limit to $\bar{\theta}_{13}$ for the detectors considered at the different facilities is approximately $\bar{\theta}_{13} \sim 1^\circ$ (a precise determination of the sensitivity limit is not available for every detector/facility). We have restricted ourselves to two possible values of the input phase $\bar{\delta}$, namely $\bar{\delta} = 90^\circ$ and $\bar{\delta} = 0$. These values represent two extreme cases, i.e. no leptonic CP-violation and maximal leptonic CP-violation. A general analysis using our method for different $\bar{\delta}$ values can be easily carried out using the results of section 3 and of appendix A.

4.2.1 The intrinsic and the sign clone flow

In figure 2 we present the clone flow for the intrinsic (left) and the sign (right) degeneracies. The clone locations have been computed for variable input parameter $\bar{\theta}_{13}$ in the range $\bar{\theta}_{13} \in [0.1^\circ, 10^\circ]$ and fixed $\bar{\delta} = 90^\circ$ (upper plots) or for a fixed value, $\bar{\theta}_{13} = 1^\circ, \bar{\delta} = 90^\circ$ (lower plots), on the verge of the sensitivity limit. Again the arrows indicate the direction of the flows from large to small $\bar{\theta}_{13}$. In figure 3 we present the same flows for $\bar{\delta} = 0$. In each figure the results for the four facilities are presented together, in order to show how the combination of two or more of them can help solving that specific degeneracy. We illustrate the outcome of our analysis by studying the two degenerations one by one.

- *The intrinsic clone*

  1. Figures 2*a*/2*c*: $\bar{\delta} = 90^\circ$

     The SB flow shows a small $\Delta\theta_{13}$-shift and $\delta \to 180^\circ$ for decreasing $\bar{\theta}_{13}$. This behaviour can be understood from eq. (3.9) and eq. (3.10) for the intrinsic clone in vacuum (this limit is indeed a good approximation for the SB facility, being $L = 130$ Km): for $\bar{\delta} = 90^\circ$, the $\Delta\theta_{13}$-shift is $\mathcal{O}[(I_2/I_1)^2]$; in the limit of small $\bar{\theta}_{13}$, we get $\sin\delta \to 0, \cos\delta \to -1$, and thus $\delta \to 180^\circ$. The results for the BB flow can be understood in the same way, with the only difference in that $(I_2/I_1)_{BB}$ is larger than $(I_2/I_1)_{SB}$.

     Regarding the Neutrino Factory setup, it can be seen that the NFG flow is well separated from the NFS flow for any value of $\bar{\theta}_{13}$. The golden channel combined with the silver and/or the SB/BB facilities is always, in principle, capable to solve the intrinsic ambiguity (i.e. provided that the corresponding experimental samples are all statistically significant and that systematic errors under control).

  2. Figures 3*a*/3*c*: $\bar{\delta} = 0^\circ$

     For the BB/SB flows we get from eqs. (3.11)–(3.12) $\tan\delta \propto \sin\bar{\delta}$. The clustering of clones at $\delta = 0$ or $\delta = 180^\circ$ for these two facilities is clearly visible in figure 3a. The NFG flow shows that all clones fall in a localized region around $\Delta\theta_{13} \sim 1.5^\circ, \delta \sim -180^\circ$, in perfect agreement with the results of [7]. The NFS flow shows the biggest $\theta_{13} - \delta$ correlation and it approaches $\delta = \bar{\delta}$ for $\bar{\theta}_{13} < 1^\circ$. The same conclusions as for $\bar{\delta} = 90^\circ$ apply: combining NFG with any one of the three other facilities should solve the intrinsic ambiguity.

- *The sign clone*

  1. Figures 2*b*/2*d*: $\bar{\delta} = 90^\circ$

     With respect to the intrinsic case we get two flow branches for each facility, each branch starting for $\bar{\theta}_{13} < 2^\circ$ except for the NFG flows that start for an even lower value of $\bar{\theta}_{13}$. This can be interpreted as a consequence of a good (theoretical) sensitivity to matter effects (i.e. to the Δm^2_{23} sign) of the different facilities and in particular of the NFG with a $L = 2810$ Km baseline. Be aware,

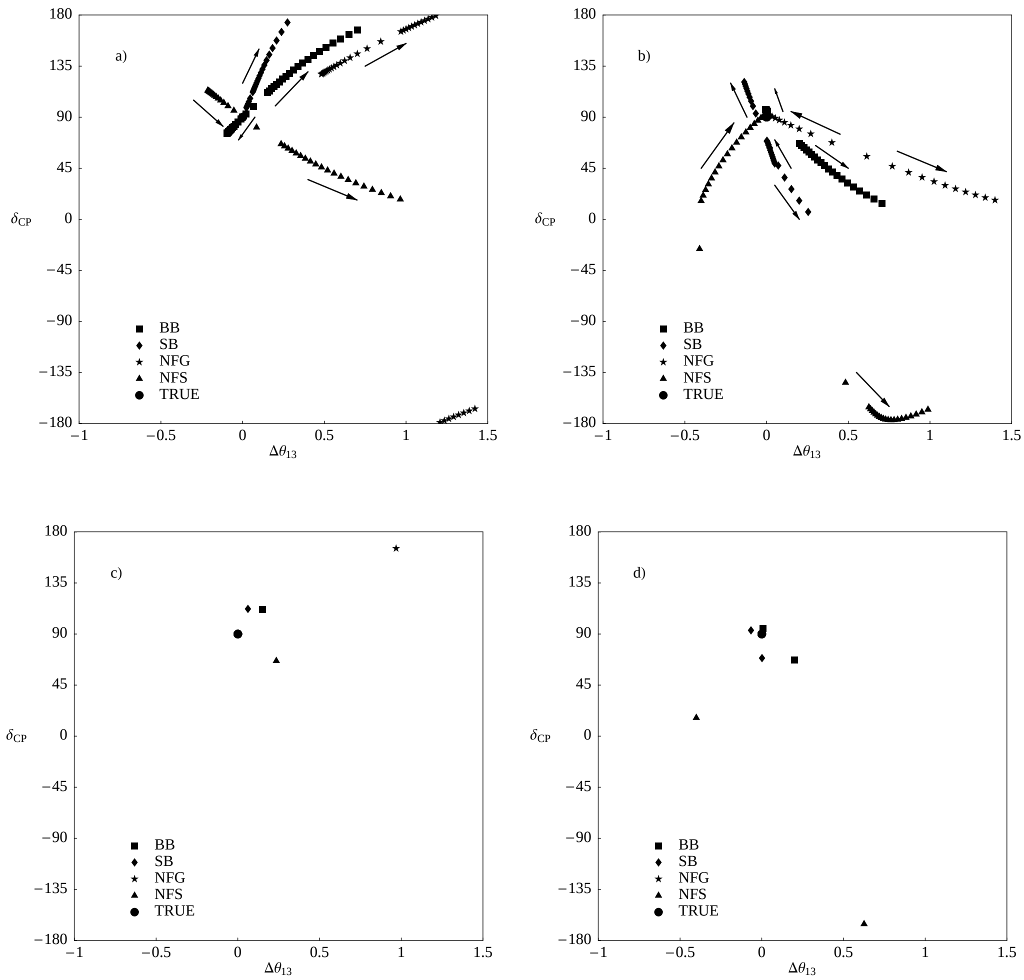

Figure 2: Clone location in the $(\Delta\theta_{13}, \delta)$ plane for the intrinsic and sign degeneracies: BB (boxes); SB (diamonds); NFG (stars) and NFS (triangles). The full circle is the true solution, $\Delta\theta_{13} = 0, \bar{\delta} = 90°$. Pictures (a) and (b) represent the intrinsic and sign clone flows for $\bar{\theta}_{13} \in [0.1°, 10°]$ and fixed $\bar{\delta}$. Pictures (c) and (d) represent the intrinsic and sign clone location for $\bar{\theta}_{13} = 1°$.

however, that in a realistic experimental case a clone could appear even when theoretically no clone is found due to statistical and systematical uncertainties.

The Golden and Silver Neutrino Factory flows are quite separated. There could be some superposition between the four flows for certain values of $\bar{\theta}_{13}$ (e.g. NFG and NFS flows in the limit of vanishing $\bar{\theta}_{13}$). Nevertheless this superposition occurs in a region nearby the true solution where the existence of a clone is somewhat irrelevant. The combination of either NFG or NFS with the SB or the BB signals should easily solve the ambiguity.[4]

In figure 2d we plot the sign clone location for $\bar{\theta}_{13} = 1°$. In this specific case

[4]Notice that for large $\bar{\theta}_{13}$ angles even the Golden channel alone can solve the sign ambiguity being strongly sensitive to matter effects.

JHEP06(2004)011

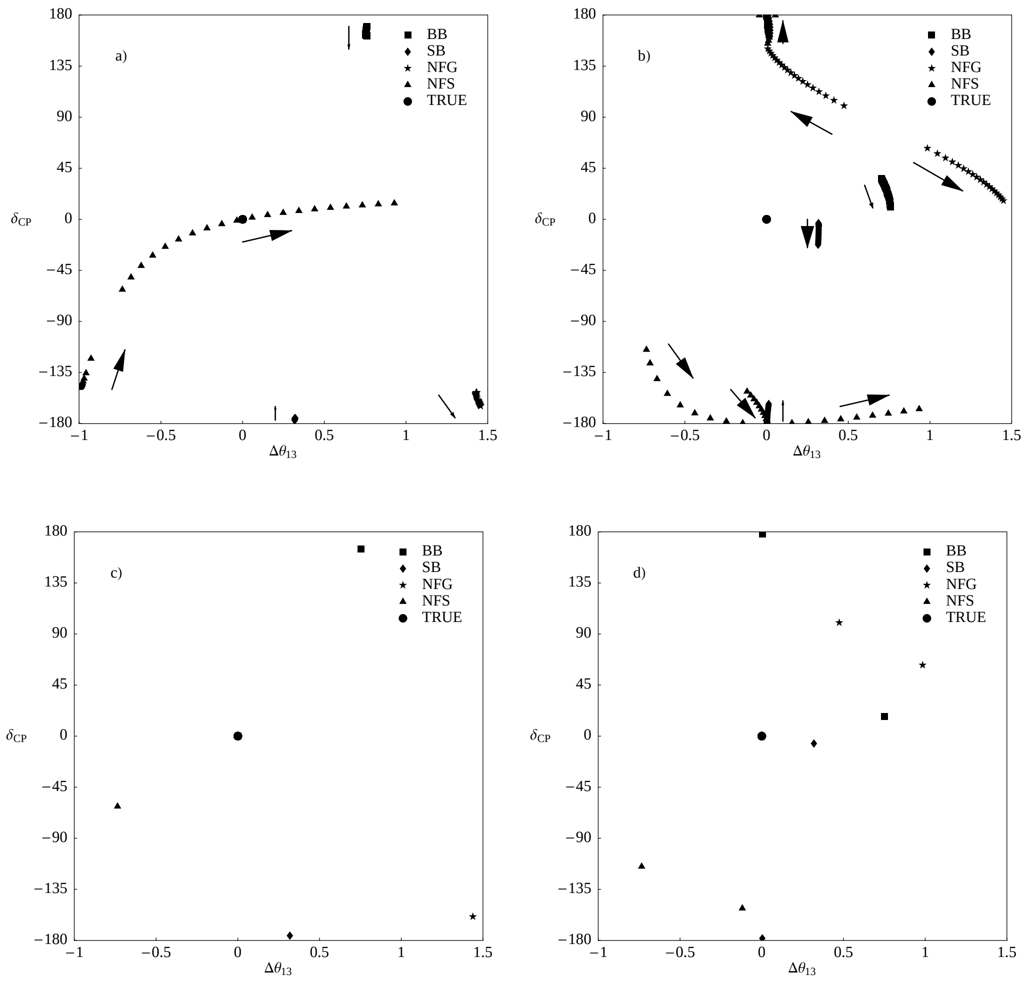

Figure 3: Clone location in the $(\Delta\theta_{13}, \delta)$ plane for the intrinsic and sign degeneracies: BB (boxes); SB (diamonds); NFG (stars) and NFS (triangles). The full circle is the true solution, $\Delta\theta_{13} = 0, \bar{\delta} = 0°$. Pictures (a) and (b) represent the intrinsic and sign clone flows for $\bar{\theta}_{13} \in [0.1°, 10°]$ and fixed $\bar{\delta}$. Pictures (c) and (d) represent the intrinsic and sign clone location for $\bar{\theta}_{13} = 1°$.

no NFG clones were found pointing out that, at least theoretically, this facility alone can solve the sign degeneracy for $\bar{\theta}_{13}$ in the atmospheric regime. Notice that the SB and BB clones lie very near. A combination of them is therefore not suited to solve the sign degeneracy for very low $\bar{\theta}_{13}$.

As a final comment we point out that the results for the sign clone for the SB and BB flows are in good agreement with the theoretical analysis of section 3.2. In vacuum, we expect the same $\Delta\theta_{13}$ shift as in the intrinsic case with $\delta_{\rm sign} = \pi - \delta_{\rm int}$. This is indeed the case by looking at figure 2a and figure 2b.

2. Figures 3b/3d: $\bar{\delta} = 0°$

   Also in this case we get two branches starting for $\bar{\theta}_{13} < 2°$ for each facility. The combination of the NFG with NFS or one of BB/SB can solve the ambiguity.

JHEP06(2004)011

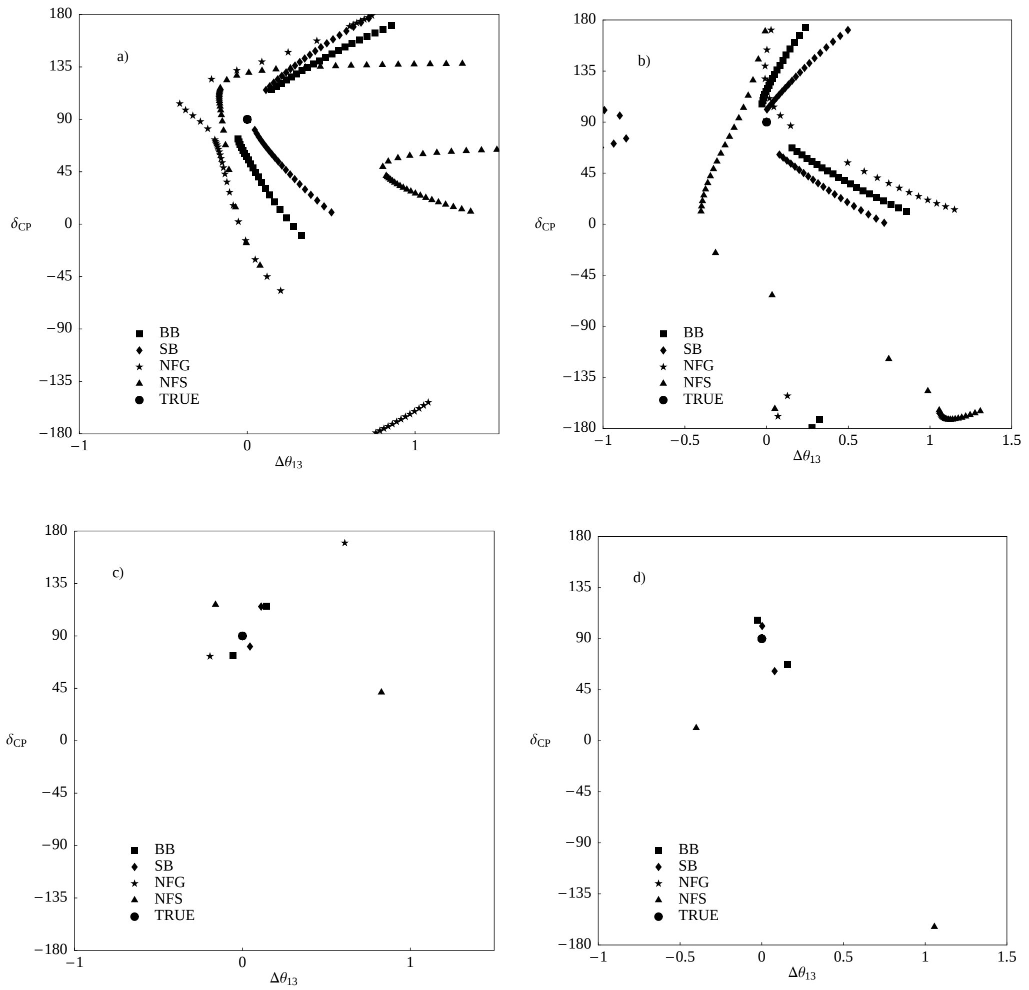

Figure 4: Clone location in the $(\Delta\theta_{13}, \delta)$ plane for the octant and mixed degeneracies: BB (boxes); SB (diamonds); NFG (stars) and NFS (triangles). The full circle is the true solution, $\Delta\theta_{13} = 0, \bar{\delta} = 90°$. Pictures (a) and (b) represent the octant and mixed clone flows for $\bar{\theta}_{13} \in [0.1°, 10°]$ and fixed $\bar{\delta}$. Pictures (c) and (d) represent the octant and mixed clone location for $\bar{\theta}_{13} = 1°$. The results have been computed with $\theta_{23} = 40°$.

Notice that for very low $\bar{\theta}_{13}$ ($\bar{\theta}_{13} \sim 0.1°$) it seems possible that a clone at $\Delta\theta_{13} \sim 0, \delta \sim 180°$ will persist. However, this value is well below the limit of the sensitivity to $\bar{\theta}_{13}$ for the considered facilities.

4.2.2 The octant and the mixed clones

If θ_{23} were maximal no additional degeneracies would be present. Otherwise two further degeneracies do appear.[5] In figure 4 we present the clone flow for the octant (left) and the mixed (right) degeneracies. The clone locations have been computed for variable input

[5]Remind, however, that these clones should probably appear also for maximal θ_{23} once including the unavoidable experimental error band.

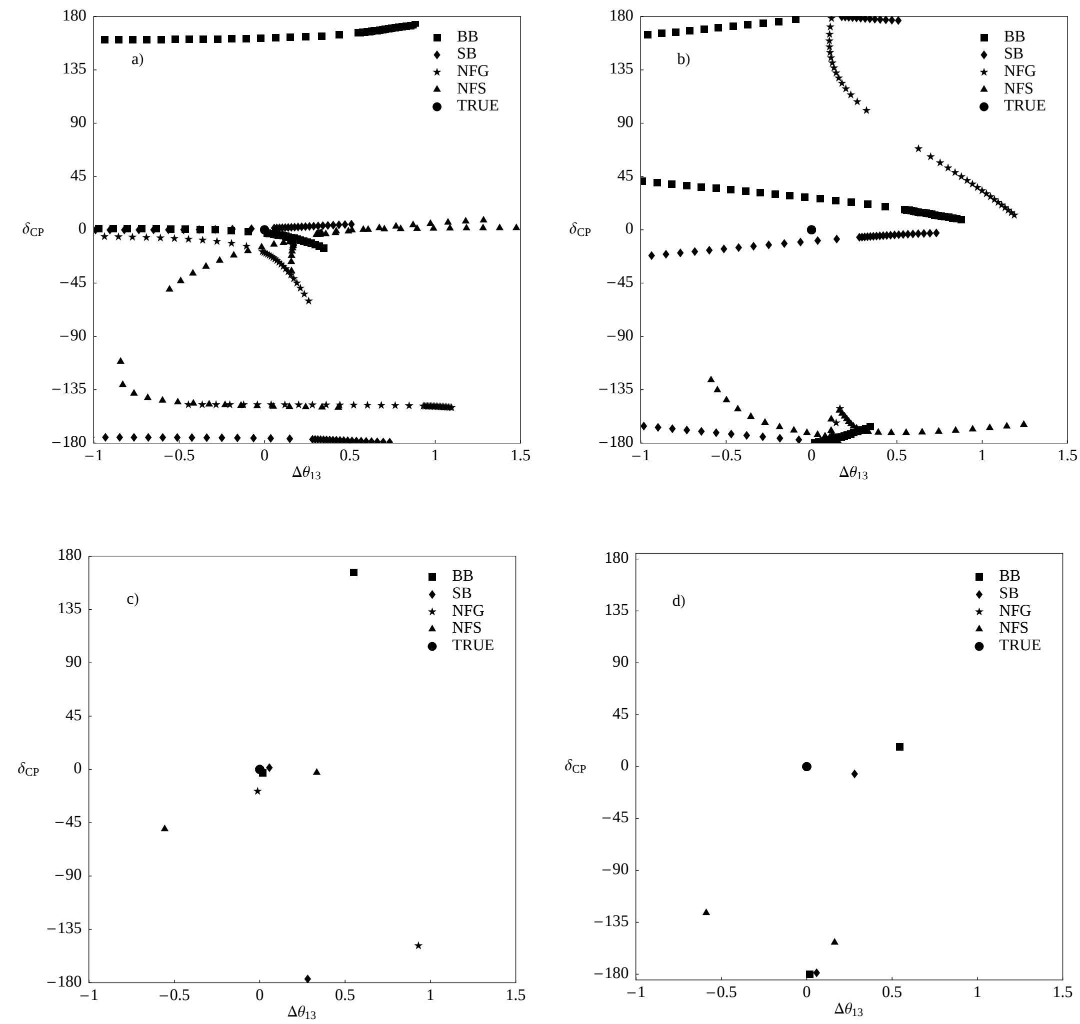

Figure 5: Clone location in the $(\Delta\theta_{13}, \delta)$ plane for the octant and mixed degeneracies: BB (boxes); SB (diamonds); NFG (stars) and NFS (triangles). The full circle is the true solution, $\Delta\theta_{13} = 0, \bar{\delta} = 0^\circ$. Pictures (a) and (b) represent the octant and mixed clone flows for $\bar{\theta}_{13} \in [0.1^\circ, 10^\circ]$ and fixed $\bar{\delta}$. Pictures (c) and (d) represent the octant and mixed clone location for $\bar{\theta}_{13} = 1^\circ$. The results have been computed with $\theta_{23} = 40^\circ$.

parameter $\bar{\theta}_{13}$ in the range $\bar{\theta}_{13} \in [0.1^\circ, 10^\circ]$ and fixed $\bar{\delta} = 90^\circ$ (upper plot) or for a fixed value, $\bar{\theta}_{13} = 1^\circ, \bar{\delta} = 90^\circ$ (lower plots). In figure 5 we present the same flows for $\bar{\delta} = 0$. In each figure the results for the four facilities are presented together.

As a general comment, we remark that the BB and SB flows for the octant and mixed degeneracies lie always very near. This is a consequence of the beam design. In [13] it was proposed to run the SPL and the BetaBeam at the same time and using the same detector located at $L = 130$ Km. In view of solving the octant and mixed degeneracies, this does not seem the optimal option: the combination of these two facilities will still be affected by these ambiguities.

- *The mixed clone*

  1. Figures $4b/4d$: $\bar{\delta} = 90°$

     Many of the features of the sign clones can be observed in the mixed case: we generically identify two branches of clone flows for each facility starting for $\bar{\theta}_{13} < 3° - 4°$, with the exception of the NFG flow that starts for $\bar{\theta}_{13} < 1°$. Looking at figure 4d for $\bar{\theta}_{13} = 1°$, we see that BB (boxes) and SB (diamonds) clones are almost superimposed, with a very small $\Delta\theta_{13}$ shift. The two NFS clones are well separated from the BB/SB pairs. Finally, as it was the case for the sign ambiguity, no NFG mixed clones appear for this specific $\bar{\theta}_{13}$.
  2. Figures $5b/5d$: $\bar{\delta} = 0°$

     In figure 5b we notice that the two BB/SB flows show very little $\theta_{13} - \delta$ correlation, drawing two stripes with very large $\Delta\theta_{13}$-shift and $\delta \sim 0, 180°$. This is again a consequence of $\tan\delta \propto \sin\bar{\delta}$ in the vacuum approximation. The two NFG/NFS branches show a larger $\theta_{13} - \delta$ correlation, with flows approaching $\delta = 0, 180°$ for decreasing $\bar{\theta}_{13}$.

- *The octant clone*

  1. Figures $4a/4c$: $\bar{\delta} = 90°$

     This is certainly the most difficult degeneracy to solve, since the flows of the four facilities overlap in a significant region of the $(\Delta\theta_{13}, \delta)$ plane, figuure $4a$. It seems feasible to reduce the overall ambiguity by combining NFG and NFS or BB/SB facilities, as it can be seen in figure $4c$. A complete elimination of this degeneracy can perhaps be achieved combining the NFG, NFS and one of the BB/SB experiments.
  2. Figures $5a/5c$: $\bar{\delta} = 0°$.

     In this case the situation seems a bit easier, with respect to the $\bar{\delta} = 90°$ case previously discussed. Indeed, the two branches of each facility cluster around the two stripes at $\delta \sim 0, 180°$ with very large spread in $\Delta\theta_{13}$.

5. Conclusions

In this paper we derive the theoretical location of the so-called "clones" that appear in the simultaneous measurement of θ_{13} and δ. The general technique used to write analytical formulæ for the clone location for the four degeneracies (called *intrinsic, sign, octant* and *mixed*) has been reported. Our analytical results apply to equiprobability and equal-number-of-events (ENE) curves as well. However, we have shown that the clone location computed from equiprobability or ENE curves can differ significantly for narrow band beam experiments. Notice that the latter approach reproduces the experimental situation, where the signal is represented by charged leptons in the detector and not by the oscillation probability itself. Using theoretical information from the equiprobability curves could thus lead to largely wrong conjectures. For this reason, in the actual calculation we presented results obtained using the ENE curves. In the paper we have considered atmospheric, solar and matter parameters as fixed quantities chosen at their present best fit values. Errors

JHEP06(2004)011

on these parameters for $\theta_{23} = 45^\circ$ and positive $\Delta m^2_{\rm atm}$ have been included in [7, 24]: the results of [7] show that the measure of $\bar\theta_{13}$ and $\bar\delta$ is strongly affected by the atmospheric and matter parameter uncertainties, respectively. Solar parameters uncertainties seem to introduce smaller errors for relatively large $\bar\theta_{13}$, whilst should probably become the most important source of error in the solar regime, $\bar\theta_{13} \leq 1^\circ$.

Several experiment synergies and/or comparison have been considered in the recent literature to handle the problem of parameter degeneracies when measuring θ_{13} or θ_{13}, δ: superbeams combination (see, for example, [25]-[27]), reactors and or vs. superbeams (see [28, 29]), or others. We decided to focus in this paper on two specific facility combinations, the Neutrino Factory plus the SPL superbeam [14, 15] and the SPL superbeam plus the Beta Beam [13], using as a reference the CERN proposal for a SuperBeam, a BetaBeam and a Neutrino Factory. In the case of the Neutrino Factory two different detectors have been considered to take care of the "golden" and "silver" channel; for the SB/BB combination, a single detector located at $L = 130$ Km is used for both beams. These facilities represent in some sense the ultimate neutrino oscillation facilities to study leptonic CP-violation. We remind, however, that the method presented in section 3 and the formulæ of appendix A can be applied to any other detector/beam setup, once computed the corresponding integrals in eq. (2.7).

Our results show that the SuperBeam/BetaBeam combination considered in [13], for this specific choice of oscillation parameters, seems to be less effective than the Neutrino Factory/SuperBeam combination to solve the eightfold-degeneracy. We have shown that, for example, the octant and mixed clone solutions for the BB/SB facilities lie always very near. The combination of the Neutrino Factory golden and silver channel, on the other hand, seems to help significantly to reduce ambiguities. In our theoretical analysis, indeed, the intrinsic, sign and mixed clone flows for NFG and NFS lie well apart for $\bar\theta_{13} \geq 1^\circ$. As a general comment, we deduce that the combination of the NF golden channel with either the NF silver channel or with one of the pair BB/SB could in principle solve these three ambiguities.

This is not the case for the octant clones. Although a significant reduction of the degeneracy can be attained combining the NFG with the NFS or with one of BB/SB, it seems that a complete elimination of the octant clones can be achieved only by combining the three facilities, NFG, NFS and BB/SB. Nevertheless, even using the combination of all the available facilities is quite possible that the experimental uncertainties will not permit to solve completely the octant ambiguity for small values of $\bar\theta_{13}$. The ultimate sensitivity of the future neutrino experiments to δ is therefore strongly dependent on the success or failure in solving it. Adding other informations (e.g. using the Minos OA proposal [23] for a SuperBeam) can probably be of great help in solving the octant clone.

Acknowledgments

We thank B. Gavela, J. Gomez-Cadenas, P. Hernandez and P. Migliozzi for useful discussions. D.M. acknowledges the European Community's Human Potential Programme under contract HPRN-CT-2000-00149 Physics at Colliders for finacial supports.

A. The analytic clone location in matter

In this appendix we generalize the treatment given for the intrinsic clone in section 3.1 to a generic case where the discrete variables $s_{\rm atm}$ and $s_{\rm oct}$ can assume different values between left and right hand side of eqs. (2.9)–(2.12).

Using eq. (3.13) and eq. (3.14) we get:

$$
\begin{aligned}
\sin\delta &= \frac{C'_1 \sin^2 2\bar\theta_{13} - C_1 \sin^2 2\theta_{13}}{\cos\theta_{13}\sin 2\theta_{13}} + \left[C'_2\cos\bar\delta + D'_3\sin\bar\delta\right] g(\theta_{13},\bar\theta_{13}) + C'_4 h'(\theta_{13}) \\
\cos\delta &= \frac{D'_1 \sin^2 2\bar\theta_{13} - D_1 \sin^2 2\theta_{13}}{\cos\theta_{13}\sin 2\theta_{13}} + \left[D'_2\cos\bar\delta + C'_3\sin\bar\delta\right] g(\theta_{13},\bar\theta_{13}) + D'_4 h'(\theta_{13})\,,
\end{aligned}
\tag{A.1}
$$

where, using a notation as much resembling as possible that of the intrinsic case, we have defined the following coefficients:

$$
\left\{
\begin{aligned}
C_1 &= \left[\frac{I_1^+ I_2^- - I_1^- I_2^+}{I_3^+ I_2^- + I_3^- I_2^+}\right] \\
C'_1 &= \left[\frac{\bar I_1^+ I_2^- - \bar I_1^- I_2^+}{I_3^+ I_2^- + I_3^- I_2^+}\right] \\
C'_2 &= \left[\frac{\bar I_2^+ I_2^- - \bar I_2^- I_2^+}{I_3^+ I_2^- + I_3^- I_2^+}\right] \\
C'_3 &= \left[\frac{\bar I_3^+ I_3^- - \bar I_3^- I_3^+}{I_3^+ I_2^- + I_3^- I_2^+}\right] \\
C'_4 &= \left[\frac{\bar I_4^+ I_2^- - \bar I_4^- I_2^+}{I_3^+ I_2^- + I_3^- I_2^+}\right]
\end{aligned}
\right.
\qquad
\left\{
\begin{aligned}
D_1 &= \left[\frac{I_1^+ I_3^- + I_1^- I_3^+}{I_3^+ I_2^- + I_3^- I_2^+}\right] \\
D'_1 &= \left[\frac{\bar I_1^+ I_3^- + \bar I_1^- I_3^+}{I_3^+ I_2^- + I_3^- I_2^+}\right] \\
D'_2 &= \left[\frac{\bar I_2^+ I_3^- + \bar I_2^- I_3^+}{I_3^+ I_2^- + I_3^- I_2^+}\right] \\
D'_3 &= \left[\frac{\bar I_3^+ I_2^- + \bar I_3^- I_2^+}{I_3^+ I_2^- + I_3^- I_2^+}\right] \\
D'_4 &= \left[\frac{\bar I_4^+ I_3^- + \bar I_4^- I_3^+}{I_3^+ I_2^- + I_3^- I_2^+}\right]
\end{aligned}
\right.
\tag{A.2}
$$

Notice that in vacuum all the coefficients of the C-type vanish.[6] Using the discrete transformation properties of the integrals I_j of table 1 we derive the corresponding transformation properties for the C_i and D_i coefficients, reported in table 2. The θ_{23}-octant transformation does not affect any of the C'_i or D'_i coefficients, but only C_1 and D_1 that are multiplied by $\cot^2\theta_{23}$ when $\theta_{23} \to \pi/2 - \theta_{23}$. The effect of an $s_{\rm atm}$ change is much stronger: all coefficients are affected by this change. The $\bar C'_i$ and $\bar D'_i$ coefficients are obtained by the $C'_{1,2,3}, D'_{1,2,3}$ in eq. (A.2) by changing $I_2^\pm \to -\bar I_2^\mp$ and $I_3^\pm \to \bar I_3^\mp$.

We present hereafter the explicit analytic solution for the θ_{13}-shift for the octant and sign clones. Inserting these results in one of eqs. (A.1) the δ-shift can be extracted. We do not present here the corresponding expression for the mixed clone.

[6]This is strictly true when considering the scenario of section 3 (identical $\nu - \bar\nu$ fluxes and constant cross-section). However, for facilities where the fluxes strongly differ, or the cross-section is rapidly increasing (such as in the case of conventional low-energy beams and superbeams or low-γ Beta-beams), it can be shown that the relation $C_i, C'_i \ll D_i, D'_i$ still holds for short baseline.

JHEP06(2004)011

	Intrinsic	Octant	Sign	Mixed
C_1	$\bar{C}_1$	$\cot^2\theta_{23}\,\bar{C}_1$	$-\bar{C}_1$	$-\cot^2\theta_{23}\,\bar{C}_1$
C'_1	$\bar{C}_1$	$\bar{C}_1$	$\bar{C}'_1$	$\bar{C}'_1$
C'_2	0	0	$\bar{C}'_2$	$\bar{C}'_2$
C'_3	0	0	$\bar{C}'_3$	$\bar{C}'_3$
C'_4	$\bar{C}_4$	$\bar{C}_4$	$-\bar{C}_4$	$-\bar{C}_4$
D_1	$\bar{D}_1$	$\cot^2(\theta_{23})\,\bar{D}_1$	$-\bar{D}_1$	$-\cot^2(\theta_{23})\,\bar{D}_1$
D'_1	$\bar{D}_1$	$\bar{D}_1$	$\bar{D}'_1$	$\bar{D}'_1$
D'_2	1	1	$\bar{D}'_2$	$\bar{D}'_2$
D'_3	1	1	$\bar{D}'_3$	$\bar{D}'_3$
D'_4	$\bar{D}_4$	$\bar{D}_4$	$-\bar{D}_4$	$-\bar{D}_4$

Table 2: Transformation laws of the coefficients C_1, C'_i and D_1, D'_i under the discrete ambiguities in the θ_{23} octant and in the Δm^2_{23} sign.

A.1 The octant clone

Using table 2, we get for the θ_{13}-shift for the octant clone the following expression:

$$\begin{aligned}
\sin^2 2\theta_{13} = {} & \sin^2 2\bar{\theta}_{13} + \left\{ \frac{\tan^2\theta_{23}}{\bar{C}_1^2+\bar{D}_1^2} \left[\left(\bar{C}_1 \sin\bar{\delta} + \bar{D}_1\cos\bar{\delta}\right)\sin 2\bar{\theta}_{13} + \frac{1}{2}\tan^2\theta_{23} \right] - \right. \\
& \left. - \left(1-\tan^2\theta_{23}\right)\left(\sin^2 2\bar{\theta}_{13} - \tan^2\theta_{23}\frac{\bar{C}_1\bar{C}_4+\bar{D}_1\bar{D}_4}{\bar{C}_1^2+\bar{D}_1^2}\right)\right\} \pm \\
& \pm \frac{\tan^2\theta_{23}}{\sqrt{\bar{C}_1^2+\bar{D}_1^2}} \left\{ \frac{1}{\bar{C}_1^2+\bar{D}_1^2}\left[\left(\bar{C}_1 \sin\bar{\delta} + \bar{D}_1\cos\bar{\delta}\right)\sin 2\bar{\theta}_{13} + \frac{1}{2}\tan^2\theta_{23}\right]^2 \right. \\
& \qquad - \left(1-\tan^2\theta_{23}\right)\left[\sin^2 2\bar{\theta}_{13} - \tan^2\theta_{23}\frac{\bar{C}_1\bar{C}_4+\bar{D}_1\bar{D}_4}{\bar{C}_1^2+\bar{D}_1^2}\right] - \\
& \qquad - 2(1-\tan^2\theta_{23}) \times \\
& \qquad \times \left[\left(\bar{C}_4\sin\bar{\delta} + \bar{D}_4\cos\bar{\delta}\right) - \right. \\
& \qquad \quad \left. - \frac{(\bar{C}_1\bar{C}_4+\bar{D}_1\bar{D}_4)(\bar{C}_1\sin\bar{\delta}+\bar{D}_1\cos\bar{\delta})}{\bar{C}_1^2+\bar{D}_1^2}\right]\sin 2\bar{\theta}_{13} - \\
& \qquad \left. - (1-\tan^2\theta_{23})^2\left[(\bar{C}_4^2+\bar{D}_4^2) - \frac{(\bar{C}_1\bar{C}_4+\bar{D}_1\bar{D}_4)^2}{\bar{C}_1^2+\bar{D}_1^2}\right]\right\}^{1/2}
\end{aligned}$$

It can be easily shown that in the vacuum limit, when $C_1, C'_i \to 0$, this equation reduces to the vacuum solution, eq. (3.20). Moreover, for $\theta_{23} \to 45°$ reduces to the general solution in matter, eq. (3.7), for the intrinsic clone.

JHEP06(2004)011

A.2 The sign clone

Using table 2, we get for the θ_{13}-shift for the sign clone the following expression:

$$\begin{aligned}
\sin^2 2\theta_{13} = & -\left(\frac{\bar{C}_1\bar{C}'_1+\bar{D}_1\bar{D}'_1}{\bar{C}_1^2+\bar{D}_1^2}\right)\sin^2 2\bar{\theta}_{13}+\frac{1}{2\left(\bar{C}_1^2+\bar{D}_1^2\right)}\times \\
& \times\left[1-2\left(\bar{C}_1\bar{C}'_2+\bar{D}_1\bar{D}'_2\right)\cos\bar{\delta}\sin 2\bar{\theta}_{13}-2\left(\bar{C}_1\bar{D}'_3+\bar{D}_1\bar{C}'_3\right)\sin\bar{\delta}\sin 2\bar{\theta}_{13}\right]\pm \\
& \pm\frac{1}{2\left(\bar{C}_1^2+\bar{D}_1^2\right)}\times \\
& \times\left\{\left[1-4\left(\bar{C}_1\bar{C}'_2+\bar{D}_1\bar{D}'_2\right)\cos\bar{\delta}\sin 2\bar{\theta}_{13}+4\left(\bar{C}_1\bar{C}'_3+\bar{D}_1\bar{D}'_3\right)^2\cos^2\bar{\delta}\sin^2 2\bar{\theta}_{13}\right]-\right. \\
& \quad -4\left[\left(\bar{C}_1\bar{C}'_3+\bar{D}_1\bar{D}'_3\right)^2+\left(\bar{C}_1\bar{C}'_1+\bar{D}_1\bar{D}'_1\right)\right]\sin^2 2\bar{\theta}_{13}- \\
& \quad -4\left(\bar{C}_1\bar{D}'_1-\bar{D}_1\bar{C}'_1\right)^2\sin^4 2\bar{\theta}_{13}- \\
& \quad -8\left(\bar{C}_1\bar{D}'_1-\bar{D}_1\bar{C}'_1\right)\times \\
& \quad \times\left[\left(\bar{C}_1\bar{D}'_2-\bar{D}_1\bar{C}'_2\right)\cos\bar{\delta}+\left(\bar{C}_1\bar{C}'_3-\bar{D}_1\bar{D}'_3\right)\sin\bar{\delta}\right]\sin^3 2\bar{\theta}_{13}- \\
& \quad -4\left(\bar{C}_1\bar{D}'_2+\bar{D}_1\bar{C}'_2\right)^2\cos^2\bar{\delta}\sin^2 2\bar{\theta}_{13}- \\
& \quad -8\left(\bar{C}_1\bar{D}'_2-\bar{D}_1\bar{C}'_2\right)\left(\bar{C}_1\bar{C}'_3-\bar{D}_1\bar{D}'_3\right)\sin\bar{\delta}\cos\bar{\delta}\sin^2 2\bar{\theta}_{13}- \\
& \quad \left.-4\left(\bar{C}_1\bar{D}'_3+\bar{D}_1\bar{C}'_3\right)\sin\bar{\delta}\sin 2\bar{\theta}_{13}\right\}^{1/2}.
\end{aligned} \tag{A.3}$$

One can verify that eq. (A.3) reduces to the vacuum solution, eq. (3.19). The first term in the square root goes to a perfect square; the second vanishes for an exact cancellation between $(\bar{D}_1\bar{D}'_3)^2$ and $\bar{D}_1\bar{D}'_1$, since in vacuum $\bar{D}'_1 \to -\bar{D}_1, \bar{D}'_2 \to -1$ and $\bar{D}'_3 \to 1$. All other terms in the square root trivially vanish since are multiplied by some C-type coefficient that goes to zero in the vacuum limit.

References

[1] B. Pontecorvo, *Mesonium and antimesonium*, *Sov. Phys. JETP* **6** (1957) 429; *Neutrino experiments and the question of leptonic-charge conservation*, *Sov. Phys. JETP* **26** (1968) 984;
Z. Maki, M. Nakagawa and S. Sakata, *Remarks on the unified model of elementary particles*, *Prog. Theor. Phys.* **28** (1962) 870;
B. Pontecorvo, V.N. Gribov and B. Pontecorvo, *Neutrino astronomy and lepton charge*, *Phys. Lett.* **B 28** (1969) 493.

[2] C. Yanagisawa, *Atmospheric neutrinos*, talk at NOON2003, `http://www-sk.icrr.u-tokyo.ac.jp/noon2003/`.

[3] SNO collaboration, Q.R. Ahmad et al., *Direct evidence for neutrino flavor transformation from neutral-current interactions in the sudbury neutrino observatory*, *Phys. Rev. Lett.* **89** (2002) 011301 [`nucl-ex/0204008`]; *Measurement of day and night neutrino energy spectra at sno and constraints on neutrino mixing parameters*, *Phys. Rev. Lett.* **89** (2002) 011302 [`nucl-ex/0204009`];
SNO collaboration, A.B. McDonald et al., AIP Conf. Proc. **646** (2003) 43.

JHEP06(2004)011

[4] KamLAND collaboration, K. Eguchi et al., *First results from KamLAND: evidence for reactor anti-neutrino disappearance*, *Phys. Rev. Lett.* **90** (2003) 021802 [hep-ex/0212021].

[5] A. Donini, M.B. Gavela, P. Hernandez and S. Rigolin, *Neutrino mixing and CP-violation*, *Nucl. Phys.* **B 574** (2000) 23 [hep-ph/9909254].

[6] M. Apollonio et al., *Search for neutrino oscillations on a long base-line at the chooz nuclear power station*, *Eur. Phys. J.* **C 27** (2003) 331 [hep-ex/0301017].

[7] J. Burguet-Castell, M.B. Gavela, J.J. Gomez-Cadenas, P. Hernandez and O. Mena, *On the measurement of leptonic CP-violation*, *Nucl. Phys.* **B 608** (2001) 301 [hep-ph/0103258];
J. Burguet-Castell and O. Mena, *Leptonic CP-violation at the neutrino factory*, hep-ph/0108109.

[8] H. Minakata and H. Nunokawa, *Exploring neutrino mixing with low energy superbeams*, *J. High Energy Phys.* **10** (2001) 001 [hep-ph/0108085].

[9] V. Barger, D. Marfatia and K. Whisnant, *Breaking eight-fold degeneracies in neutrino CP-violation, mixing and mass hierarchy*, *Phys. Rev.* **D 65** (2002) 073023 [hep-ph/0112119].

[10] G.L. Fogli and E. Lisi, *Tests of three-flavor mixing in long-baseline neutrino oscillation experiments*, *Phys. Rev.* **D 54** (1996) 3667 [hep-ph/9604415].

[11] A. Cervera et al., *Golden measurements at a neutrino factory*, *Nucl. Phys.* **B 579** (2000) 17 [hep-ph/0002108].

[12] P. Huber, M. Lindner and W. Winter, *Superbeams versus neutrino factories*, *Nucl. Phys.* **B 645** (2002) 3 [hep-ph/0204352];
P. Huber and W. Winter, *Neutrino factories and the 'magic' baseline*, *Phys. Rev.* **D 68** (2003) 037301 [hep-ph/0301257];
W. Winter, *Resolving degeneracies for different values of $\theta_1 3$*, hep-ph/0308227.

[13] P. Zucchelli, *A novel concept for a anti-$\nu/e/\nu/e$ neutrino factory: the beta beam*, *Phys. Lett.* **B 532** (2002) 166;
J. Bouchez, M. Lindroos and M. Mezzetto, *Beta beams: present design and expected performances*, hep-ex/0310059.

[14] J. Burguet-Castell, M.B. Gavela, J.J. Gomez-Cadenas, P. Hernandez and O. Mena, *Superbeams plus neutrino factory: the golden path to leptonic CP-violation*, *Nucl. Phys.* **B 646** (2002) 301 [hep-ph/0207080].

[15] A. Donini, D. Meloni and P. Migliozzi, *The silver channel at the neutrino factory*, *Nucl. Phys.* **B 646** (2002) 321 [hep-ph/0206034];
A. Donini, D. Meloni and P. Migliozzi, *The $\nu/e \to \nu/\tau$ channel as a tool to solve ambiguities*, *J. Phys.* **G 29** (2003) 1865 [hep-ph/0209240];
A. Donini, *Using $\nu/e \to \nu/\tau$: golden and silver channels at the neutrino factory*, hep-ph/0305247;
A. Donini, *NUFACT'03: the fate of the clones*, hep-ph/0310014.

[16] D. Autiero et al., *The synergy of the golden and silver channels at the neutrino factory*, *Eur. Phys. J.* **C 33** (2004) 243 [hep-ph/0305185].

[17] M. Freund, *Analytic approximations for three neutrino oscillation parameters and probabilities in matter*, *Phys. Rev.* **D 64** (2001) 053003 [hep-ph/0103300].

JHEP06(2004)011

[18] H. Minakata, H. Nunokawa and S.J. Parke, *CP and t trajectory diagrams for a unified graphical representation of neutrino oscillations*, *Phys. Lett.* **B 537** (2002) 249 [hep-ph/0204171]; *Parameter degeneracies in neutrino oscillation measurement of leptonic CP and t violation*, *Phys. Rev.* **D 66** (2002) 093012 [hep-ph/0208163].

[19] P. Migliozzi and F. Terranova, *Next generation long baseline experiments on the path to leptonic CP-violation*, *Phys. Lett.* **B 563** (2003) 73 [hep-ph/0302274].

[20] A. Cervera, F. Dydak, J. Gomez Cadenas, *A large magnetic detector for the neutrino factory*, *Nucl. Instrum. Meth. A* **451** (2000) 123.

[21] CERN WORKING GROUP ON SUPER BEAMS collaboration, J.J. Gomez-Cadenas et al., *Physics potential of very intense conventional neutrino beams*, hep-ph/0105297.

[22] M. Apollonio et al., *Oscillation physics with a neutrino factory*, hep-ph/0210192.

[23] D. Ayres et al., *Letter of intent to build an off axis detector to study $\nu_\mu \to \nu_e$ oscillations with the NuMI neutrino beam*, M. Diwan et al., NuMI-NOTE-SIM-0714.

[24] M. Koike, T. Ota and J. Sato, *Ambiguities of theoretical parameters and CP/T violation in neutrino factories*, hep-ph/0103024.

[25] V. Barger, D. Marfatia and K. Whisnant, *How two neutrino superbeam experiments do better than one*, *Phys. Lett.* **B 560** (2003) 75 [hep-ph/0210428].

[26] P. Huber, M. Lindner and W. Winter, *Synergies between the first-generation JHF-SK and NuMI superbeam experiments*, *Nucl. Phys.* **B 654** (2003) 3 [hep-ph/0211300].

[27] H. Minakata, H. Nunokawa and S.J. Parke, *The complementarity of eastern and western hemisphere long- baseline neutrino oscillation experiments*, *Phys. Rev.* **D 68** (2003) 013010 [hep-ph/0301210].

[28] H. Minakata, H. Sugiyama, O. Yasuda, K. Inoue and F. Suekane, *Reactor measurement of $\theta_1 3$ and its complementarity to long-baseline experiments*, *Phys. Rev.* **D 68** (2003) 033017 [hep-ph/0211111]; *Exploring leptonic CP-violation by reactor and neutrino superbeam experiments*, *Phys. Lett.* **B 580** (2004) 216 [hep-ph/0309323].

[29] P. Huber, M. Lindner, T. Schwetz and W. Winter, *Reactor neutrino experiments compared to superbeams*, *Nucl. Phys.* **B 665** (2003) 487 [hep-ph/0303232].

JHEP06(2004)011